The Iraqi Journal for Mechanical and Material Engineering, Vol. 25, No. 2, June 2026.

ISSN: 1819-2076; eISSN: 2313-3783

EXPERIMENTAL AND ANALYTICAL STUDY OF FUNCTIONALLY GRADED BLENDS FOR ARTIFICIAL HIP PROSTHETIC

Enas Al-Zubaidy [1*], Ahmed Fadhil Hamza [2], Zuhair Jabbar Abdul Ameer[3]

[1,2]Department of Engineering of Polymer and Petrochemical Industries, University of Babylon, Babylon, Iraq

[3]Department of Prosthetics and Orthotics, College of Engineering, University of Kerbala, Kerbala, Iraq

***Corresponding author: E-mail: enas_talib@hilla.unc.edu.iq**

ABSTRACT

Ultra-high molecular weight polyethylene (UHMWPE) wear and bone resorption due to particle release led to hip replacement (THA) failure. This can be achieved by applying a functional gradient approach to environmentally friendly polymer blends (PLA and UHMWPE) layering and a porous layer using (PVA) with the mixture to form the top layer of PFGB. A hot press technique was used to study the structural buildup strategy of the blends. To ensure a smooth transition between the components, (UHMWPE) was used at a specific volume fraction as the core material. The wear mechanism was determined by pin-on-disc testing using Archard's wear equations. The chemical composition was analyzed by (FTIR). A comparative study was conducted using (FEM) to compare the experimental and analytical results. The study demonstrated better structural cohesion and diffusion of the blends, as well as reduced wear and abrasion rates with a volume fraction gradient. The coefficient of friction of (COF) layers improved by (4.71%, 3.64%, 3.28%, 3.6%, 1.8%, 0.05%), respectively, and the (FEM) values were in agreement with the experimental results.

Keywords: Biomaterials, Coefficient of Friction, Finite Element Model, Functionally Graded Blend, Porous Functionally Graded Blend

NOMENCLATURE

COF	Coefficient of Friction
E	Modulus
FGB	Functionally Graded Blend
ρ	Bulk density

Received: September 6, 2025. **Publisher: University of Babylon / Faculty of Engineering**

Accepted: April 14, 2026. **Journal homepage: https://www.iqjfmme.com**

υ	Poisson ratio
V_w	Volumetric wear rate
L_w	Linear wear rate
A	Area of contact
K_w	Wear coefficient
P	Body weight
PFGB	Porous Functionally Graded Blend
S	Sliding distance

1. INTRODUCTION

Advanced technologies enable highly effective analysis of the contact force strain distribution of the hip prosthesis in fracture patients to assess mechanical performance and analyze the biomechanical effects of lateral conditions and anatomical abnormalities on contact force/stress in the patient's joint for treatment planning Genda et al., [1] . The dome of the acetabulum (head), as a weight-bearing area, is virtually elastic. Therefore, it is responsible for stabilizing and contacting the femoral head under joint pressure. The ball's surface moves in a sliding motion towards the acetabulum. The lifespan of the hip joint decreases significantly. Requiring replacement due to wear and tear on the joint's contact surfaces. This wear and tear typically results from contact pressure and sliding distance caused by daily activity Laurian & Tudor[2] .

Undoubtedly, the peak of the average stress intensity was found to occur on the lateral surface of the acetabular ligament during standing at its midpoint. The peak stress was also found at the edge of the posterior horn Yoshida et al.,[3] . It is preferable to optimize the geometric design parameters, in order of importance ("Thickness associated with the acetabular cavity and also the diagonal clearance") Yew et al., [4] . Several reviews deal with medical applications of UHMWPE Bracco et al., [5,6]. UHMWPE has long been chosen for bearing surfaces because of its interlocking bonding for improved performance and durability Bistolfi et al., [7] , a high strength-to-weight ratio Nawaz Khan et al.,[8] . It boasts superior corrosion resistance, exceptionally high fracture toughness, and is known for its biocompatibility compared to other polymers Bistolfi et al.,[7] . It was reported that using a relatively large-diameter endothelial implant reduces the risk of dislocation upon exposure to trauma Kluess et al., [9] . When developing a mathematical model to evaluate the contact stress distribution in the hip, important points were found in analyzing the maximum contact stress value in relation to the hip load and the shape of the stress distribution Ipavec et al.,[10] . The diameter of the femoral head and the surgical approach play an important role in the risk of dislocation and loosening in the following primary total hip replacement (THA). The smaller the diameter of the femoral head, the lower the risk of cumulative dislocation Berry et al.,[11] . Smaller bearing femoral head diameters can enhance the stability of THA implants Sultan et al.,[12] . However, the different

mechanical properties of bones and implants cause difficulties in bone formation around prostheses. Fixations made of functionally graded blends (FGBs) have been proposed. An attempt has been made to reconstruct bone using a bone remodeling algorithm in finite element analysis. The gradient direction has a significant impact on bone remodeling and formation Genda et al.,[1,2]. Functionally graded blends, including ceramics and polymers, have been used, both of which offer lightweight, biocompatibility, and better corrosion resistance in the body compared to composites. This research aims to investigate the structure of functionally graded blends as a bone replacement material in terms of their wear capacity and stress distribution. Finite element method studies have been recognized and trusted as reliable integral tools in the analysis of human articulations. Finite element analysis (FEA) is a reliable and comprehensive analytical tool for analyzing human joints. Its key advantage lies in the precise control of loading parameters, motion, and the alignment of limit conditions with structural changes in the dynamic joint response. Furthermore, ligament forces, forces applied to the contact area (body weight), and consequently cartilage stresses are crucial outcomes for biomechanical modeling. FEA has been employed to identify and determine the causes of failure and fatigue leading to total knee replacement Morais et al., [13,14] . FEA has also been applied in various fields of biomedical engineering. Optimal design utilizes numerical algorithms tailored to optimize the design of relevant applications (American Society for Testing and Materials International ASTM International [15,16].

2. EXPERIMENTAL WORK

The matrix phase consists of ultra-high molecular weight polyethylene (UHMWPE) in the form of white granules, with a molecular weight below 1,700,000, supplied by LOBA CHEME PVT.LTD. The second phase matrix is poly lactic acid (PLA) (98% purity) in the form of a white powder, at 151°C, supplied by BASF 3D Printing Solutions BV. The matrix is reinforced with polyvinyl alcohol (PVA) to obtain a porous structure (appearance of PVA: white powder, molecular weight (1,700-1,800) originating in Germany, packed in the UK by ME Scientific Engineering LTD. Hot press theory was used to prepare samples of polymer mixtures (poly lactic acid with ultra-high molecular weight polyethylene (PLA) and polyethylene (UHMWPE). After thorough shaking in a small container, the mixture was prepared as a powder at the specified volumetric fractions (Table 1). Polyvinyl alcohol (PVA) was used at the specified volumetric fractions (Table 2). Poly lactic acid and ultra-high molecular weight polyethylene were mixed as a powder at the weight ratios calculated in Table 1 and pressed into a gauge die (185 mm × 195 mm and 4 mm deep, assuming a die tolerance of 1 mm), Figure 1 (a). The samples were pressed into the die in a heat press at 5 MPa and 175 °C and gradually cooled to room temperature. A solution (100 g of deionized water to 10 g of polyvinyl alcohol) was added. It was continuously mixed for 10 minutes using a magnetic mixer. PLA and UHMWPE powders were then added and mixed thoroughly until the components were dissolved, Excess water is usually filtered manually.

The mixture was then pressed as previously described. The experimental work involved the fabrication of six different samples (FGB and PFGB) using the powder technique, as shown in Figure 1 (b, c). After PFGB production, the blends sheets were heated to 140 c° for 10 sec and then heat-pressed about 1 MPa for one minute.

2.1. Experimental procedure

2.2.1 Characterization Techniques (Miscibility Tests)

Figure 2, shows the vibrational absorption bands at (3757 cm^{-1}) for PLA\UHMWPE, pure PLA, and pure UHMWPE, indicating the formation of 0-H bonds. A large absorption band at (3471-3417 cm^{-1}) was observed for PLA\UHMWPE, along with a small absorption band at (2924 cm-1) Maizatul et al., [18]. This is likely due primarily to the hydroxyl component and the vibration (O-H bond stretching) associated with the carbohydrate. The peaks at (3039–2854 cm^{-1}) are also attributed to the CH group. This range showed higher absorption for PLA/UHMWPE compared to the pure spectrum. which is expected given that PLA leads to the formation of (-CH2- and -CH2-) Ogata et al., [19]. For pure PLA, the carbonyl stretching absorption band was shown at (1774 cm^{-1}), and this absorption appeared to be smaller in HMWPE\PLA. The increased absorption bands at the dimer (1720-1512 cm^{-1}) are attributed to the formation of unsaturated (C = C bonds) in PLA\UHMWPE Urkaç, [14]. Similarly, for PLA at the dimer (1774-1504 cm^{-1}), the peak was sharper and broader. An absorption peak was observed at (1658 cm^{-1}) for PLA, and a smaller shift at (1620 cm^{-1}) for PLA\UHMWPE. The presence of this peak indicates the transition of the polymer surface to one poor in hydrogen and rich in interconnected carbon atoms. Furthermore, some carbonyl formation was observed at around (1720 cm^{-1}) in the absorption spectrum of PLA\UHMWPE. Vibrational absorption bands at 1685 cm^{-1} were observed for the PLA\UHMWPE blend; the bands are more intense with their shift to a lower level. This can be explained by the nature of the interaction between PLA and UHMWPE, indicating the formation of C = 0 bonds.

Figure 3, the C-H stretching bands for PLA\UHMWPE\PVA of formalin can be seen at the absorption peaks at (2924, 2845, 2762, and 2677 cm^{-1}) Morais et al., [13] . O-H stretching bands of PLA\UHMWPE\PVA are observed at (3500 cm^{-1}) where the bands are more intense with shifting to a lower level. Ester bonds were observed at the band at (1620 cm^{-1}) due to the (C-O bond), while the peaks at (1018 and 1111 cm^{-1}) indicate the presence of (C-O bond), these bands can demonstrate the formation of ester bonds during the curing process Thomas et al., [17] . It is expected that the C = O group in PLA will react with the O-H group in PVA to form hydrogen bonds. This reaction may improve the cohesion and diffusion between the three polymers without reacting with UHMWPE, Figure 4.

2.2.2. Wear and Friction Properties of FGBs and PFGBs

Wear and friction test was achieved according to ASTM G99-05 ASTM International[15] using the machine of pin-on-disc U.S.A MT4003 version 10 micro-test. The dimensional samples were of 20 mm long ,10 mm width, and 3 mm thickness was sliding against a steel

(16 Mn Cr5), pin of D = 6 mm, the hardness ("of sphere HRC 56, and surface roughness R = 3.2 μm") in a vertical configuration with load 7N. The pin was sliding in a track of D = 12 mm of a speed 250 (rpm) and sliding distance (200) m. The wear specimen shown in Figure 5, the images prepared samples in Table 1.

Wear and debris from daily activities and walking are an important factor in implant failure. However, resizing contact stress by creating a tight surface between femoral head - acetabular cup which is critical to prolonging implant life. In a prosthetic stem specimen, ultra-high molecular weight polyethylene (UHMWPE) is a commonly used material for the bearing surface Zhang & Ren[16] . Wear tests on UHMWPE composites reveal that the material generates wear residues, which can lead to osteolysis and ultimately implant loosening. These tests also demonstrate that the size and shape of wear particles can influence the biological response ASTM International[15]. Therefore, PLA has been introduced to increase the elasticity factor. However, this study investigated the effect of functional gradients on wear progression in total hip replacements.

A plastic deformation pattern was observed along the pin trail of blend A1, as shown in Figures 6 and 7, and a shiny trail was observed due to the surface nature of the polymer, where UHMWPE is semi-crystalline, unbranched, biphasic: crystalline phase (chains folded into highly oriented sheets), and amorphous Wang et al., [20]. A1 and A2 recorded the highest coefficient of friction. It is likely that the properties of UHMWPE contributed to the plastic deformation, and its properties dominate the matrix. Blend A3 showed a decrease in coefficient of friction values with plastic deformation; the 30:70 ratio always outperforms in its properties Hussain et al.,[21] . In blends A4 and A5, the effect of increasing PLA is evident. It is likely that both UHMWPE and PLA are immiscible, and upon heating, the molecules undergo rearrangement. Due to the difference in molecular size, a structure filled with agglomerates and clusters results from gradual cooling and rearrangement. Increasing PLA promotes phase separation. Phase separation is reflected positively in the creation of a structure with protrusions and depressions. This structure reduces friction and corrosion mechanisms between bodies in a friction and corrosion environment Mao et al., [22] . Mixture B5 recorded the highest values of friction and corrosion, and in contrast, a foam structure was observed that has internal air bubbles that give the matrix lightness and enhance cellular osmosis processes in a biological environment Chuaponpat et al., [23,24]. Undoubtedly, the addition of PVA may have enhanced the smoothness of the surface under compression, resulting in the glossy, embossed appearance observed along the pin track, due to its biodegradability and hydrophilic properties. In general, the stress concentration in these porous areas may exceed their tensile strength, leading to the formation of holes. The combined effect of the high amount of PVA and the inherent physical properties of PLA and UHMWPE also reduces the overall impact resistance.

From Figure 7 (b), the overall wear rate remains high with the dominance of UHMWPE and gradually increases with increasing PLA content. Initially, the wear rate

may not change significantly because UHMWPE maintains good wear resistance while retaining some of the advantages of PLA. At higher PLA contents, the mechanical properties may begin to change due to PLA's characteristics. However, at certain levels (e.g., A4 and A5), the mixtures may reach a compositional equilibrium where the improved mechanical properties of UHMWPE and the softer properties of PLA contribute to a characteristic wear rate. For example, in the B5 wear rate, an improvement in the wear rate is observed, especially if sufficient post-treatment PVA is available to participate in a softer matrix with stress-dissipating properties. Under certain conditions (hydrophilic and film-forming), PVA reduces the overall wear rate and thus compensates for the high PLA/UHMWPE ratios. Mechanical properties, such as plasticity, toughness, and rigidity, may reach an equilibrium point Wang et al.,[25].

3. NUMERICAL METHODOLOGY

This section discusses the numerical model of the blend layers, the governing equations, the boundary conditions, and their validation. Figure 8 shows the finite element model of the blend samples (PLA\UHMWPE\PVA) to perform numerical simulation of each layer of PFGB, indicating the boundary conditions for friction and wear testing, and to make a comparison between the experimental results and numerical simulation using finite element theory. A disk with dimensions (8 mm diameter and 3 mm thickness) and dimensions of a sliding pin (1 mm cylinder diameter and 0.4 mm pin head), number of nodes (1181), and number of elements (4495) was created. Using the properties of the static structure, the contact tolerance (0-203 mm) was determined, and the mesh elements were determined using the tetrahedron method.

The numerical model of the femoral head region consists of five layers of a blends (UHMWPE\PLA) and a porous outer layer (PLA\UHMWPE\PVA) in the surface, each with a thickness of 3 mm, and the outer acetabular- cup made of the same PFGB, as shown in Figure 8. This model was assumed to be void-free between the femoral head / the liner. Finally, this model was simulated with Ansys workbench 16.1 after carefully applying all boundary conditions. The FE model of the prosthetic stem and bearing head (ball) with boundary conditions for friction and wear testing, as shown in Figure 9 (a, b). The layers of both the stem and the head base with the ball. Figure 8 (c) represents a mesh model of the stem consisting of six PFGB layers. The model consists of (8989) nodes and (14593) elements. The bearing head model is constructed from a hemisphere connected to a circular base consisting of six additional circles, each representing a layer of PFGBs for both the base and head. The base consists of (8990) nodes and (7659) elements, while the ball consists of (533) nodes and (476) elements. The diameter of the ball head decreases with the base (from 32 mm to 6 mm). The mesh was optimized for the prosthetic stem model as well as for the loading models under friction and wear conditions because mesh optimization affects the accuracy of the results, and this is consistent with Huzni et al.,[26].

3.1. Wear behavior

To estimate the wear behavior between hip implant components, the modified Archard's wear model is used to estimate the linear and volumetric wear rates between the head and shaft surfaces under different gait loading conditions using functionally graded blend compositions Di Puccio & Mattei, [27,28] . According to the modified Archard's wear law, the linear and volumetric wear rates can be calculated using Eqs. (1) and (2) respectively:

$$L_w(linear\ wear) = K_w(wear\ coeffecient) \times P(\ body\ weight) \times S(sliding\ distance) \quad (1)$$

Where L_w refers to the linear wear rate in mm; K_w refers to the wear coefficient in mm^3 N/mm; P is denotes the contact pressure in MPa; and S is the sliding distance in mm.

$$V_w(volume\ of\ wear) = L_w(linear\ wear) \times A \quad (2)$$

Where V_w refers to the volumetric wear rate in mm^3, and A represents the contact surface area of the articulating bodies (acetabular cup and femoral head) in mm^2. In this study, the linear and volumetric wear rates between the head and shaft interface were calculated considering the FGB layer material of the stem and head. The friction coefficient and wear rates were taken from experimental studies under similar dry sliding conditions as shown in Table 4. The upper interaction is between a rectangular surface with dimensions of (12 mm length, 6 mm width). Therefore, the head and stem interaction surface area are (72 mm^2) for calculating the volumetric wear. The linear and volumetric wear rates for 10 million (1.00E + 0.7) cycles will be calculated according to the formulas given in Equations (3) and (4), respectively Belwanshi et al., [29].

$$L_w = K_w \times P \times S \times 10^7\ (mm^3/10^7) \quad (3)$$

$$V_w = L_w \times A \times 10^7\ (mm^3/10^7) \quad (4)$$

3.2. Effective material properties for FGBS

An active FGB plate material's properties are assumed to change continuously along with its thickness direction. These properties are obtained using a simple power law Zhang & Ren[16] distribution or an exponential law Duc et al., [30] that calculates each FGB volume fraction. The functionally graded two-component material and its properties, as shown in Table 2, such as:- Young's modulus "E" , Poisson ratio"υ", and bulk density "ρ", were obtained using the following Eqs.(5-7) Duc et al.,[30]

$$E_{eff} = (E_1 - E_2)\left(\frac{z}{h} + \frac{1}{2}\right)^n + E_2 \quad (5)$$

$$\rho(z) = (\rho_1 - \rho_2)\left(\frac{z}{h} + \frac{1}{2}\right)^n + \rho_2 \quad (6)$$

$$v(z) = (v_1 - v_2)\left(\frac{z}{h} + \frac{1}{2}\right)^n + v_2 \quad (7)$$

To calculate the properties of the material (the porous layer), we can assume a plate with a Cartesian coordinate system(x, y, z), where x and y represent the average plane of the plate, and z represents a coordinate system whose thickness can be expressed as $(-h/2 \leq z \leq h/2)$. The total length, width, and thickness of the plate are $(a, b,$ and $h)$, respectively, as shown in Eqs. (8-10) below Torres et al., [31]:

$$P(z) = (P_1 - P_2)\left(1 + \frac{2z}{h}\right)^n + P_2 - P_{Por} \quad (8)$$

$$P_{Por} = \propto\backslash 2\left(1 - 2\left(\frac{|z|}{h}\right)\right)(P_1 + P_2) \quad (9)$$

$$\begin{bmatrix} E(z) \\ \rho(z) \end{bmatrix} = \begin{bmatrix} E_{1,2} \\ \rho_{1,2} \end{bmatrix}\left(1 + \frac{2z}{h}\right)^n + \begin{bmatrix} E_2 \\ \rho_2 \end{bmatrix} - \frac{\propto}{2}\left(1 - 2\left(\frac{|z|}{h}\right)\right)\begin{bmatrix} E_1 + E_2 \\ \rho_1 + \rho_2 \end{bmatrix} \quad (10)$$

Where porosity volume fraction is "α", $E_{1,2} = E_1 - E_2$, and $\rho_{1,2} = \rho_1 - \rho_2$, the local Poisson ratio $v(z)$ is assumed to be constant $(v(z)=v)$ as shown in Table 3.

4. RESULTS AND DISCUSSION

The magnitude and direction of the forces applied to the femoral head vary dynamically throughout the walking cycle, specifically during the standing phase. Sub-phases can be identified as initial contact, intermediate standing, and terminal standing Plank et al.,[32] .

When the linear wear rate of the artificial joint components, particularly the polyethylene, consistently exceeds a certain limit, typically referred to as 0.1 mm per year. Wear exceeding this rate is associated with a higher risk of complications leading to implant failure. Figure 10 shows the total deformation, Von Mises stress, sliding distance, pressure and frictional stress, when the layers are arranged in a functional gradient according to Figure 9, where the lowest friction rate and wear coefficient were for the blends (from A1 in the core to A5, considering B5 in the surface). It also showed the wear rate after 10, 30, 50, and 60 cycles of the finite element model. The PFGB contact region (head\ stem) for sliding distance, pressure and frictional stress that match the wear rate after 10, 30, 50, and 60 cycles of the finite element model, Figure 10. Figure 11 total

deformation, and Figure 12 von Mises stress for the PFGB layers model, which were analyzed to calculate friction and wear rates for each cycle of different walking activities. Numerical simulations showed a slight change in the magnitude of the total deformation and von Mises stresses. The higher the volume fraction of poly lactic acid, the higher the total wear rate Liu et al., [33]. This is also the case for the porous graded sample, recorded higher wear rate. As the concentration of PLA in the matrix increases, mechanical properties may deteriorate, and wear resistance may decrease Li et al., [34]. PLA generally has lower wear resistance than UHMWPE Plamadiala et al., [35], and a higher PLA content can significantly increase the wear rate Yang et al., [36], The holes act as irregularities, much like geometric cuts, causing the stress to be localized much more than the stress in the surrounding material when the load is applied. The specific parameters used in the simulation, such as sliding speed and contact time, can significantly affect the wear rate results. If these factors remain constant, however, material properties change due to differences in composition. In this study, wear rates were calculated from multiple simulations. Variations due to random processes in material behavior may result in variations that tend to increase with higher PLA content while remaining within the expected range. Figure 13 the contact pressures, sliding distances, and Fractional stress of the PFGB model, which were analytically calculated to wear rates for each cycle of different walking activities. In wear simulations of materials such as PLA and UHMWPE, these calculations are critical to understanding and predicting wear behavior.

It enhances measurements of contact conditions and material response during sliding (the total length of the sliding motion), providing accurate predictions of wear rate (the amount of material that can be removed by wear over time) and evaluating material performance (through shear stress at the contact surface, a key factor in determining frictional forces and energy dissipated during dry sliding, which can affect overall wear rates). Contact pressures are also calculated, which influence the initiation and propagation of wear mechanisms, such as scaling or abrasion. These parameters are essential inputs to wear models (such as the Archard wear model) used in this study, which provide a more comprehensive understanding of wear mechanisms and the development of more wear-resistant materials and designs.

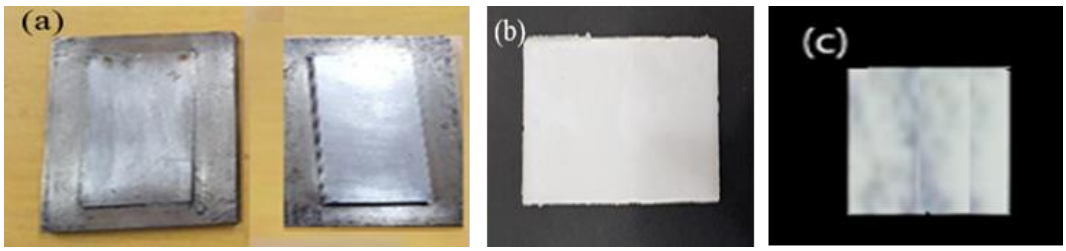

Fig. 1. (a) The steel mold (b) the sheet of FGBs, (c) the sheet of PFGBs.

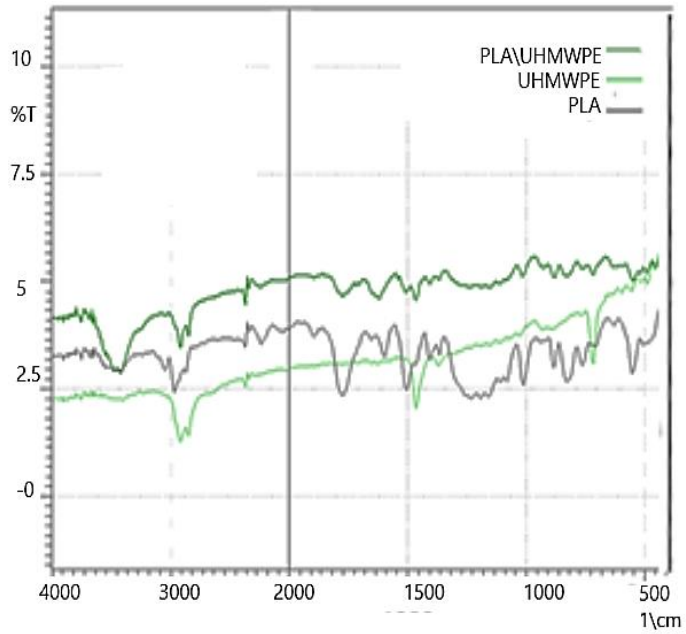

Fig. 2. FTIR micro spectra for the spectra of (PLA\UHMWPE), pure UHMWPE, and pure PLA.

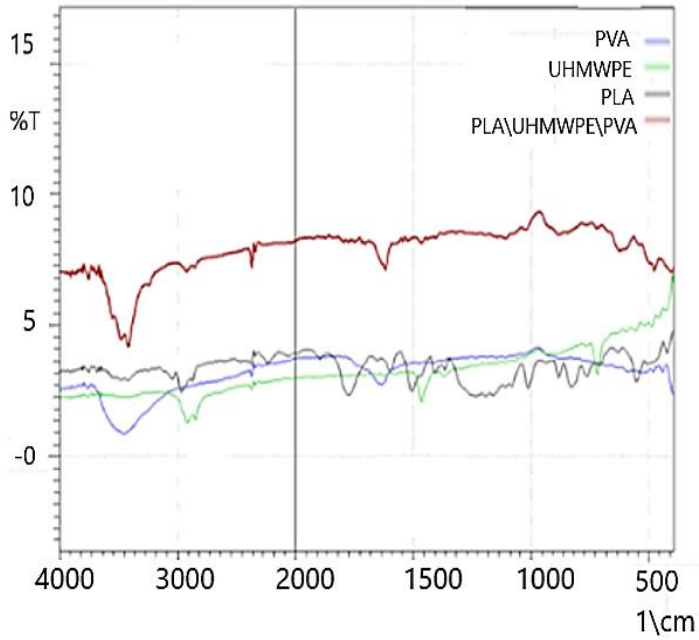

Fig. 3. FTIR microscopic for the spectrums of (PLA\UHMWPE\PVA), pure UHMWPE, pure PVA and pure PLA.

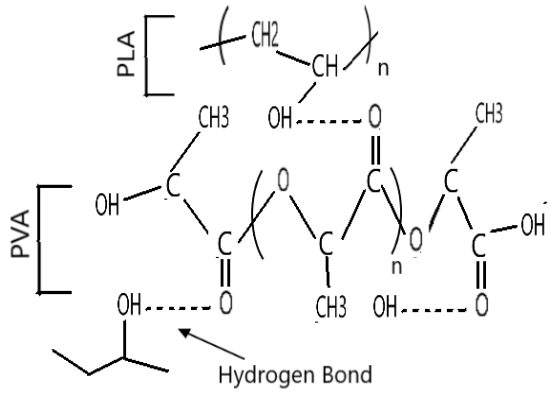

Fig. 4. The reaction of PFGBs constituents (porous layer).

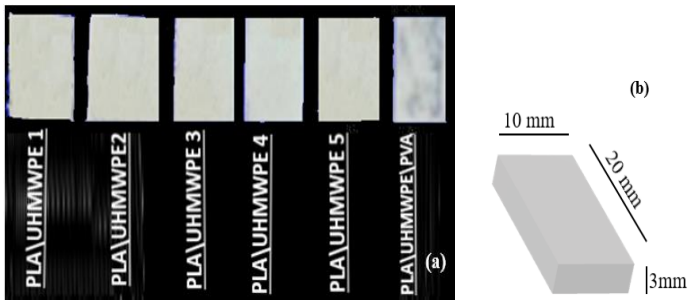

Fig. 5. (a) The wear samples test, (b) schematic diagram of FGB specimen.

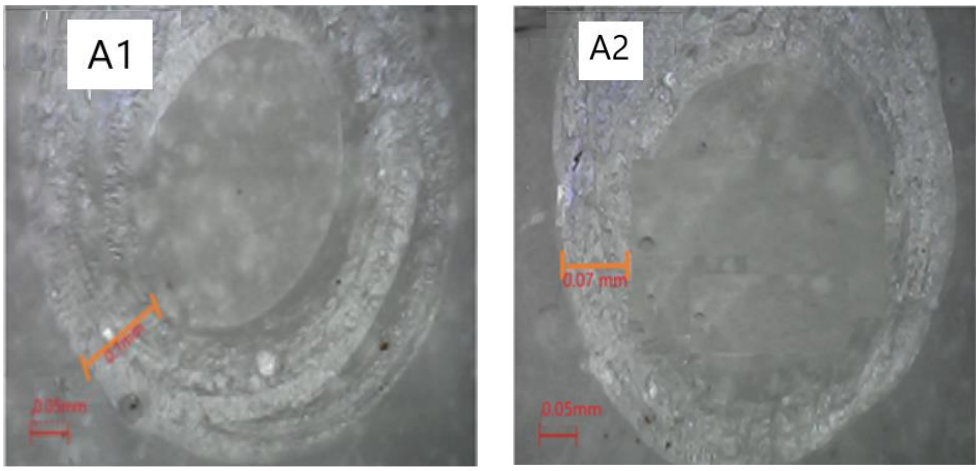

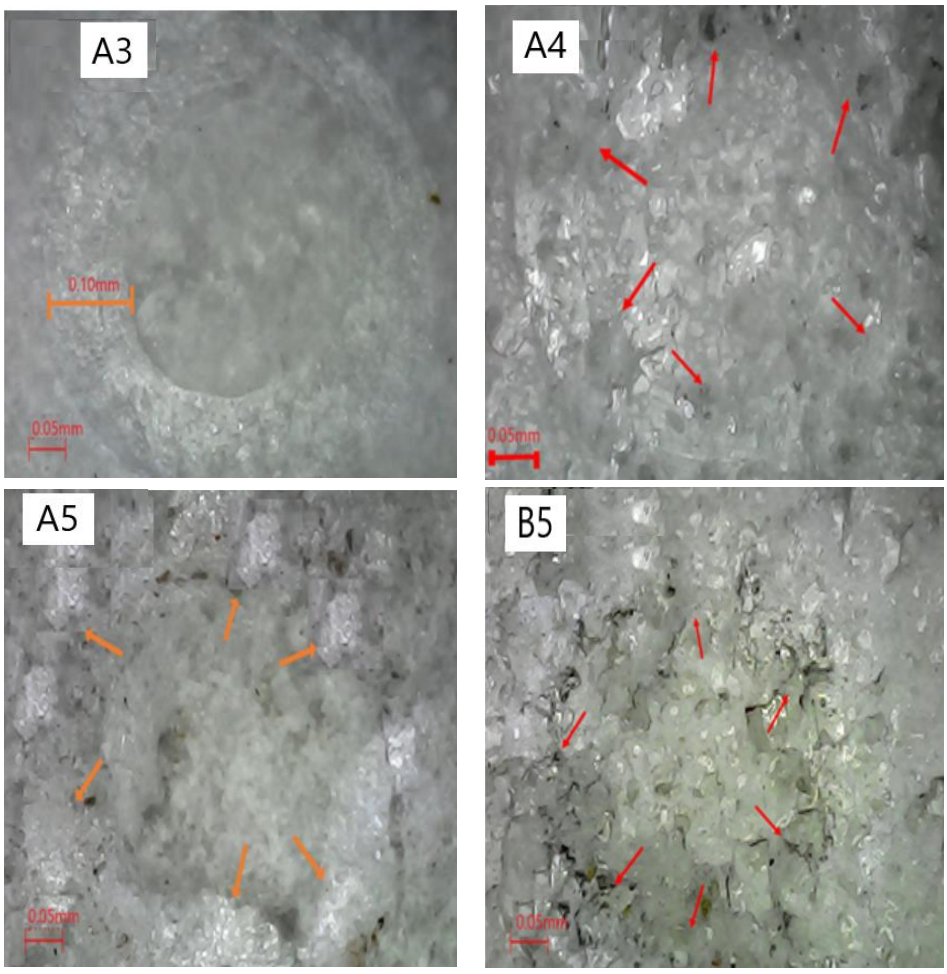

Fig. 6. Digital microscope Image for PFGBs composites materials.

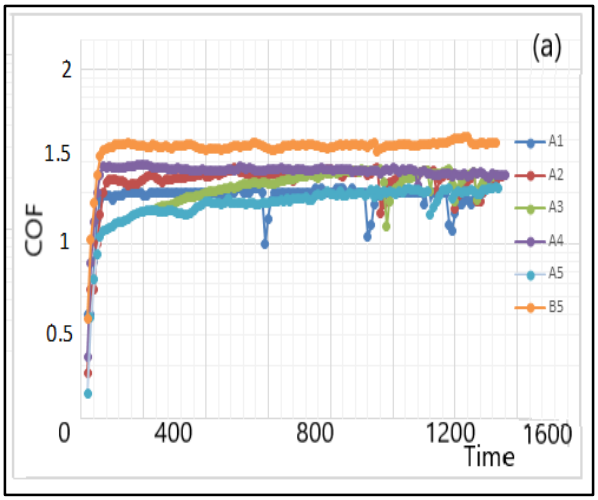

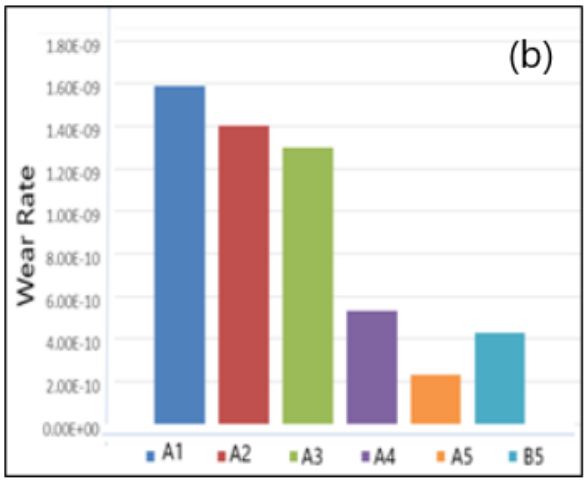

Fig. 7. Illustrate PFGBs under wear test (a) coefficient of friction vs. time, (b) wear rate.

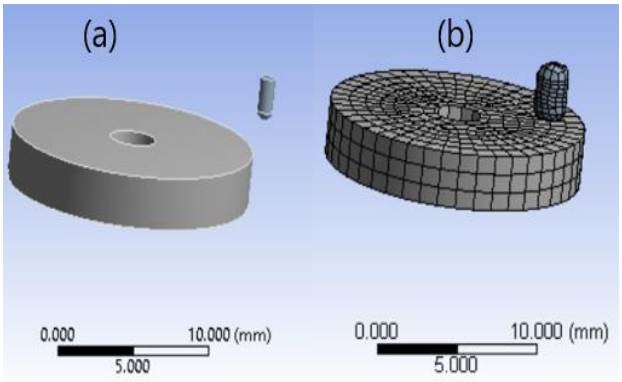

Fig. 8. (a) Finite element model, (b) meshed simples.

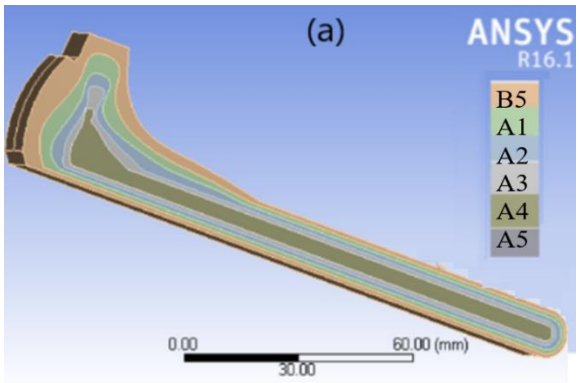

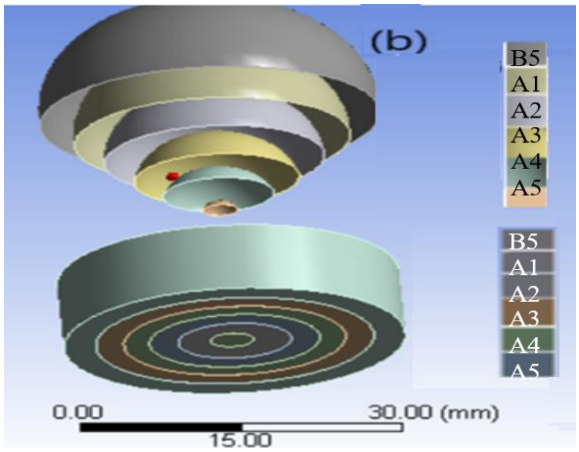

Fig. 9. Numerical model of the (a) FGB femoral prostheses, (b) acetabular cup component, (c) meshed FGB femoral prostheses

At 10 cycles.

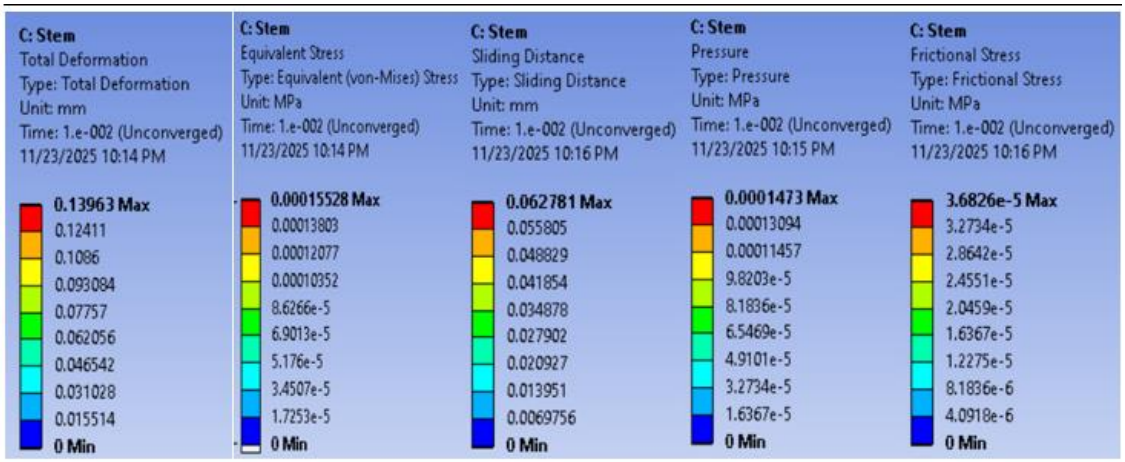

At 30 cycles

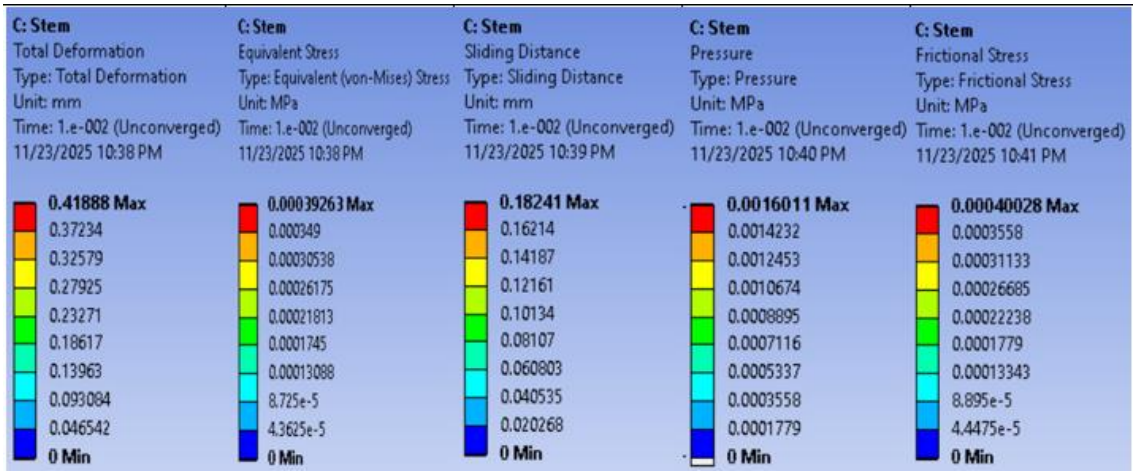

At 50 cycles

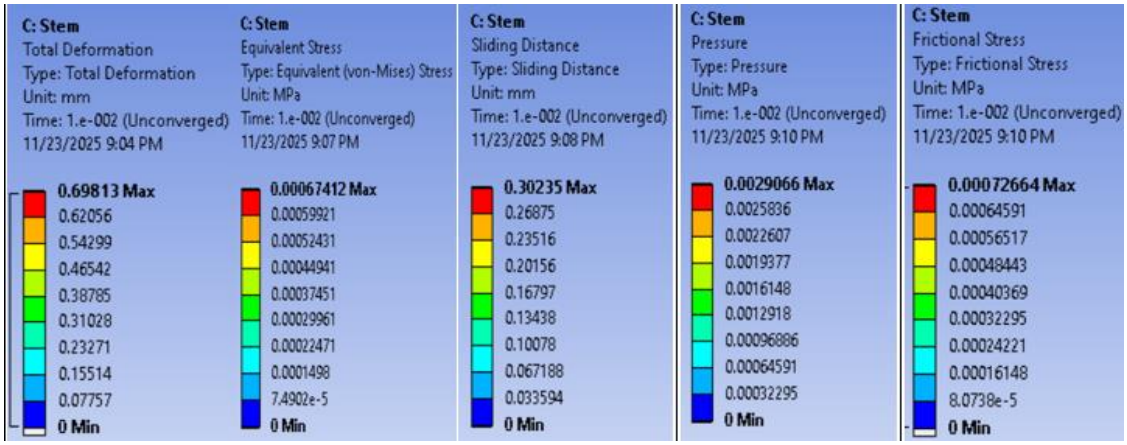

At 60 cycles

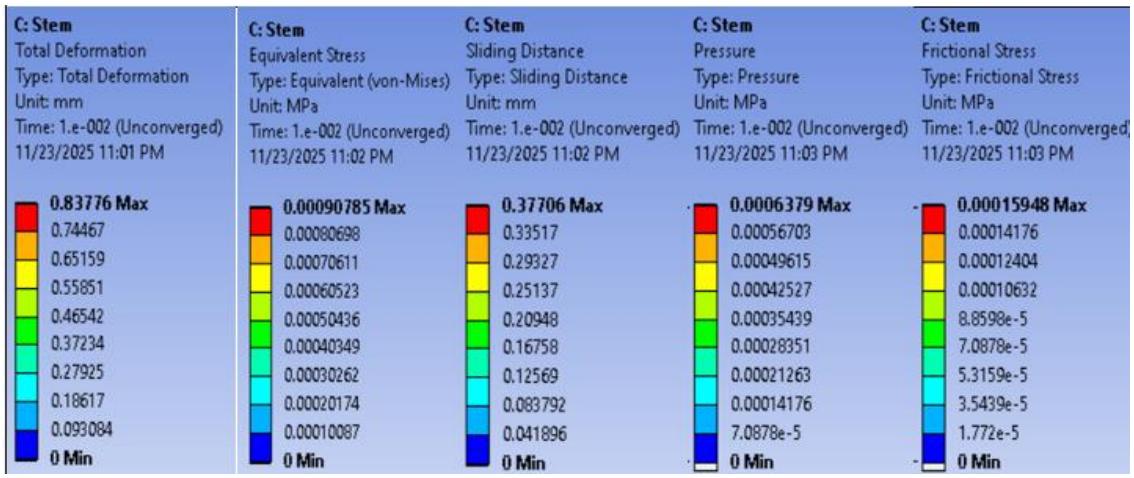

Fig. 10 Total deformation for PFGBs composites materials.

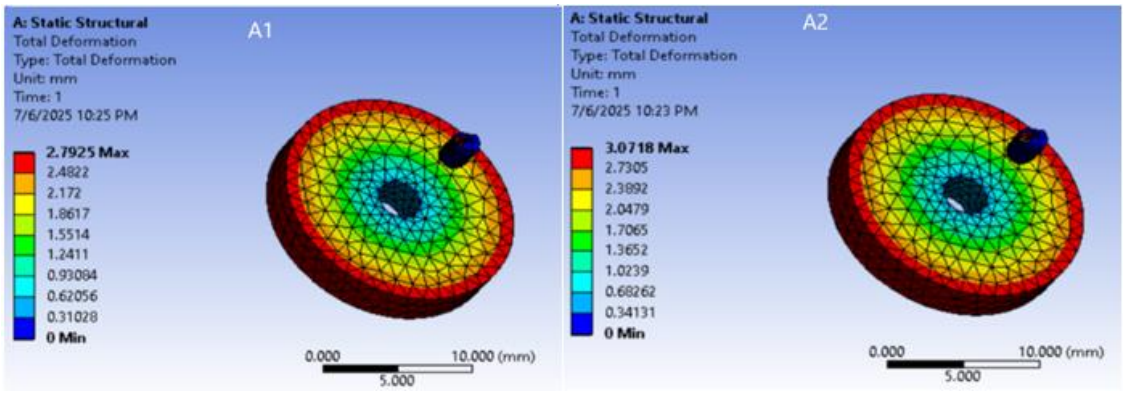

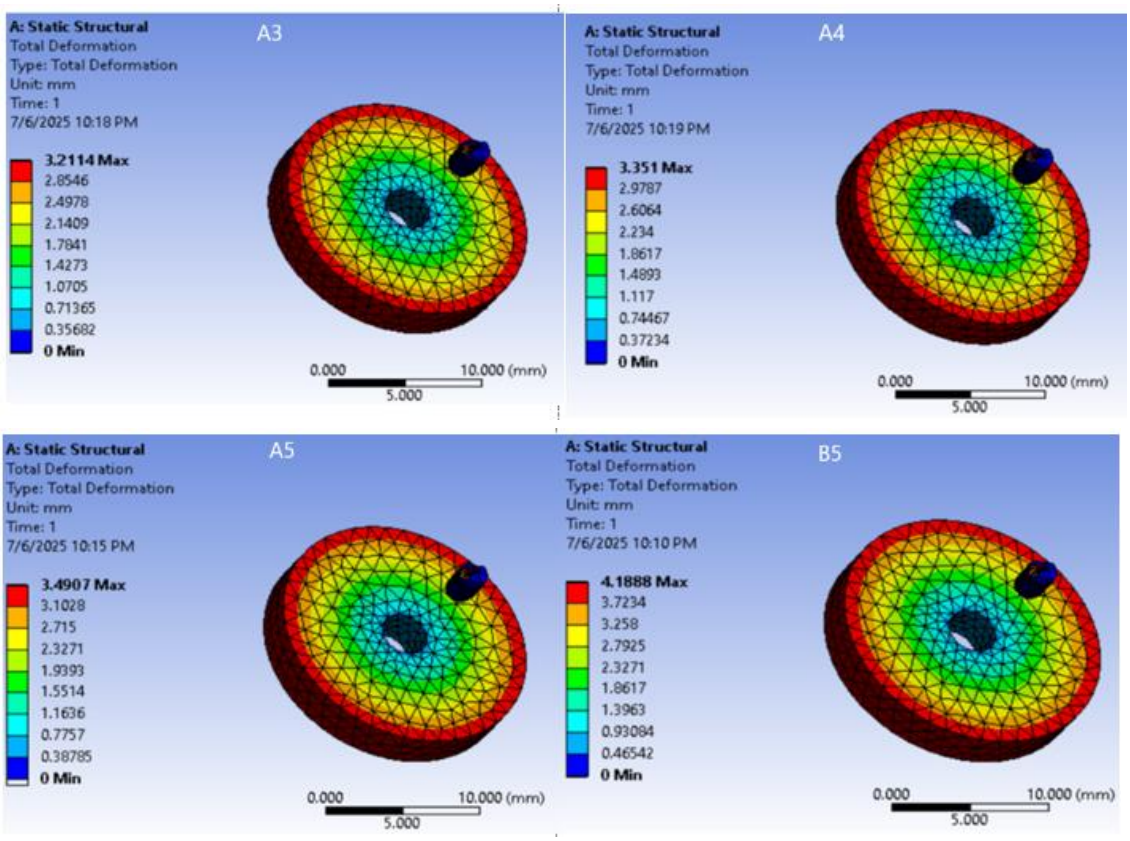

Fig. 11. Total deformation for PFGBs composites materials.

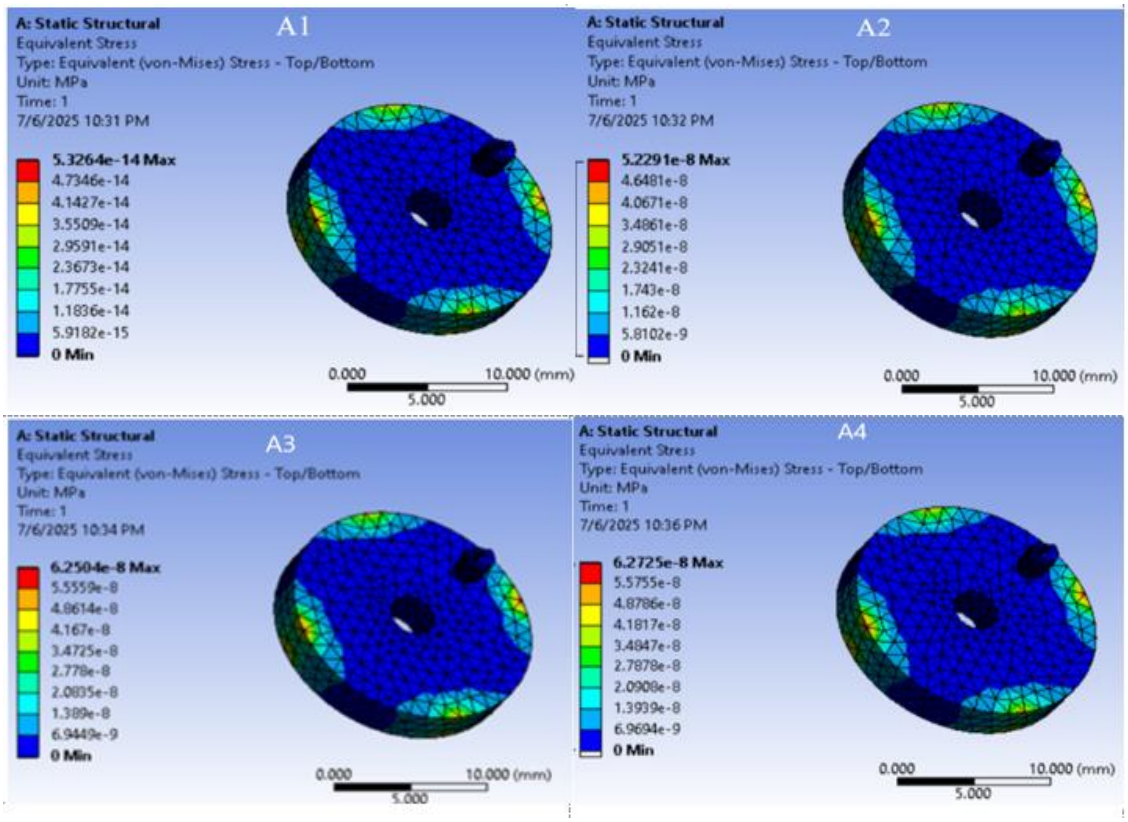

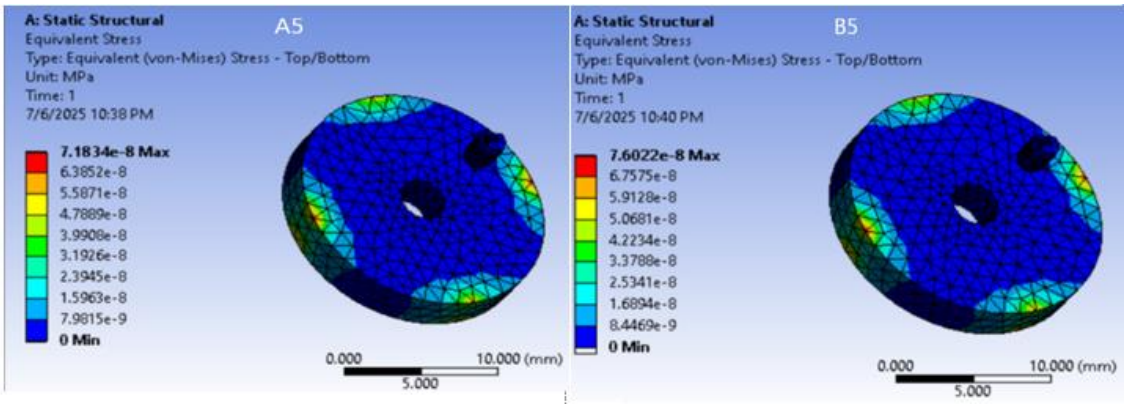

Fig. 12. Equivalent Von Mises for PFGBs blend materials.

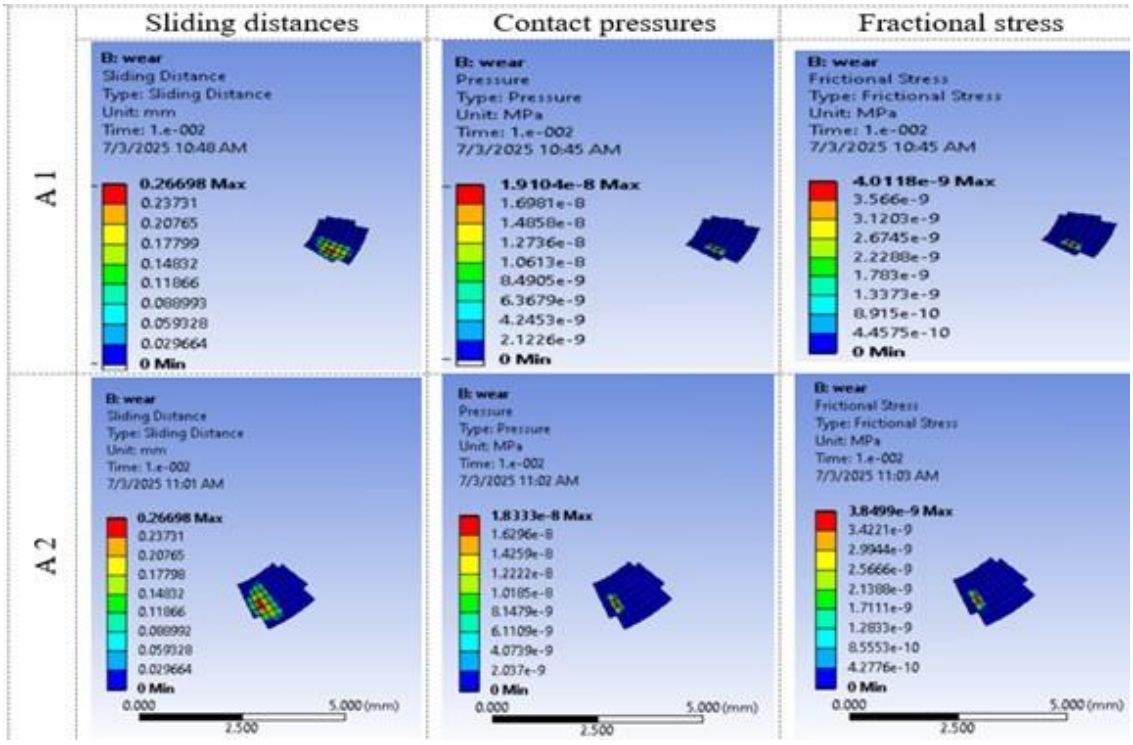

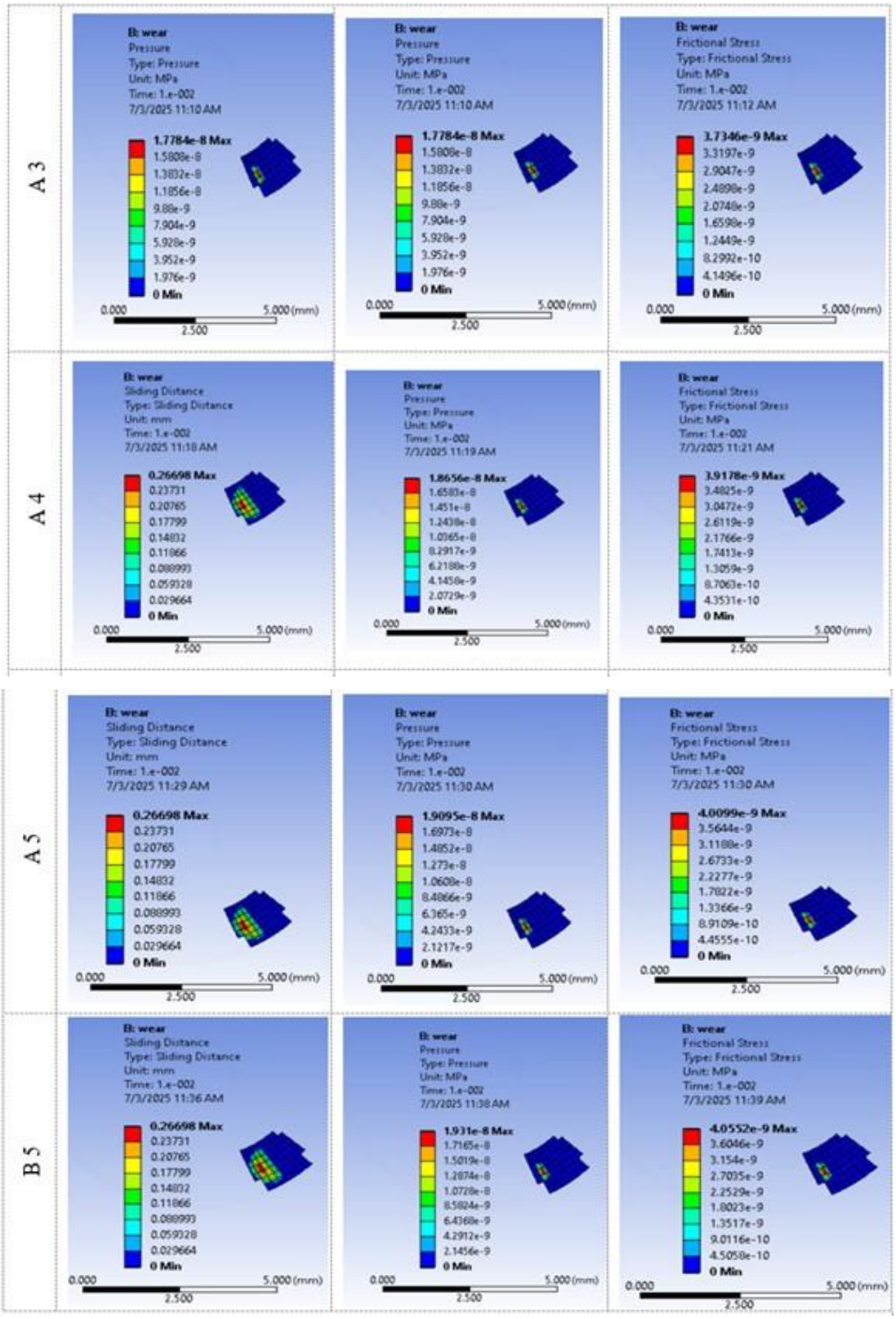

Fig. 13. Illustrate contact pressures, sliding distances and fractional stress of the PFGB layers model.

5. CONCLUSIONS

This research focused on the feasibility of using FGBP as a selective material for the production of prosthetic limb stems. The study focused on examining the friction and wear mechanisms of the selected materials individually, to reveal the unique properties of each material under dry friction, both experimentally and theoretically. The axial and translational motion of the prosthetic limb stem were also studied analytically. The results were as follows:

- The use of materials such as UHMWPE, which are similar to human bone and highly resistant to abrasion, enhances Osseo integration and prolongs the life of the implant.
- The highest coefficient of friction was recorded for B5, the lack of mechanical strength was compensated for by better resistance to fluid permeability, while A1 was less susceptible to fluid permeability and had a lower coefficient of friction compared to pure UHMWPE at 4.71%.
- The A1 and A2 alloys showed the highest friction and abrasion resistance, which makes them suitable for use after the porous layer, while the A4 and A5 alloys showed the lowest friction and abrasion resistance and are therefore suitable for use as substrates.
- The use of a blend gradation in the volume ratio reduces the uniqueness of mechanical properties and allows for the formation of structures with different properties depending on the location.
- The analytical and experimental study showed a convergence in the results. The results for the volumetric erosion rates of the layers calculated from the Archard equation are close to the experimental results obtained in Figure 7 (a).

Table 1. Volume fraction of PFGB Layers

No.	FGB Samples	PLA wt. %	UHMWPE wt. %	PVA wt. %
A1	PLA\UHMWPE 1	10	90	-
A2	PLA\UHMWPE 2	20	80	-
A3	PLA\UHMWPE 3	30	70	-
A4	PLA\UHMWPE 4	40	60	-
A5	PLA\UHMWPE 5	50	50	-
B5	PLA\UHMWPE\PVA5	25	25	50

Table 2. The properties of FGBs

Blend	Properties		
	E_{eff} (MPA)	$\upsilon(z)$	ρ (g/cm^3)
A1	49.8	0.352	1.243
A2	48.8	0.402	1.215

A3	50.4	0.346	1.264
A4	49.3	0.358	1.225
A5	52.24	0.33	1.328

Table 3. The properties of PFGB

Blend	Properties		
	E_{eff} (MPA)	$\upsilon(z)$	ρ (g/cm^3)
B5	43.6	0.27	1.108

Table 4. Summary of PFGB results

Layer	V_w	L_w
A1	3.6964×10^{-5}	2.94×10^{-5}
A2	4.04432×10^{-4}	3.22×10^{-5}
A3	4.22016×10^{-4}	3.36×10^{-5}
A4	$4.396 \times 10^{6-4}$	3.50×10^{-5}
A5	2.71296×10^{-4}	2.16×10^{-5}
B5	6.68192×10^{-4}	5.32×10^{-5}

Table 5. Summary of walking cycle

Walking cycle phase	Magnitude	Direction
Initial Contact/Loading (response (0-10%)	A sharp initial increase in force occurs, resulting in the first two peaks of the vertical ground reaction force (GRF).	The resulting force is typically directed slightly forward and outward/forward. The hip is near maximum flexion and begins to extend.
Standing Phase (approximately 60% of the walking cycle)	The foot is on the ground and bearing weight.	The majority of high-intensity forces are transmitted through the hip joint.
Intermediate Stand (10-30%)	The force temporarily decreases before rising to its second peak, which is often higher.	The body's weight is positioned parallel to the forefoot. The maximum pressure, usually of moderate intensity, is concentrated on the lateral surface of the acetabulum. The force is compressive and directed upwards.
Terminal position (30-50%)	The force reaches its maximum, which can be 2.4-2.9 times the body weight	The force is typically directed outwards and backwards toward the end of this phase (at the "foot release" or just before the swing).

REFERENCES

[1] Genda, E., Iwasaki, N., Li, G., MacWilliams, B. A., Barrance, P. J., and Chao, E. Y. " Normal hip joint contact pressure distribution in single-leg standing—effect of gender and anatomic parameters", Journal of Biomechanics, Vol. 34, No. 7, pp. 895-905, 2001. https://doi.org/10.1016/S0021-9290(01)00041-0

[2] Laurian, T., and Tudor, A. " Some aspects regarding the influence of the clearance on the pressure distribution in total hip joint prostheses", Proceeding of the National Tribology Conference RotTrib03, Galati, Romania, 2003.

[3] Yoshida, H., Faust, A., Wilckens, J., Kitagawa, M., Fetto, J., and Chao, E. Y.-S. " Three-dimensional dynamic hip contact area and pressure distribution during activities of daily living", Journal of Biomechanics, Vol. 39, No. 11, pp. 1996-2004, 2006. https://doi.org/10.1016/j.jbiomech.2005.06.026

[4] Yew, A., Jagatia, M., Ensaff, H., and Jin, Z. " Analysis of contact mechanics in McKee-Farrar metal-on-metal hip implants", Proceedings of the Institution of Mechanical Engineers, Part H: Journal of Engineering in Medicine, Vol. 217, No. 5, pp. 333-340, 2003. https://doi.org/10.1177/095441190321700501

[5]Bracco, P., Bellare, A., Bistolfi, A., and Affatato, S. " Ultra-high molecular weight polyethylene: influence of the chemical, physical and mechanical properties on the wear behavior. A review", Materials, Vol. 10, No. 7, p. 791, 2017. https://doi.org/10.3390/ma10070791

[6] Hasegawa, M., Tone, S., Naito, Y., and Sudo, A. " Ultra-high-molecular-weight polyethylene in hip and knee arthroplasties, " Materials, Vol. 16, No. 6, p. 2140, 2023. https://doi.org/10.3390/ma16062140

[7] Bistolfi, A., Giustra, F., Bosco, F., Sabatini, L., Aprato, A., Bracco, P., and Bellare, A. " Ultra-high molecular weight polyethylene (UHMWPE) for hip and knee arthroplasty: The present and the future, " Journal of Orthopaedics, Vol. 25, pp. 98-106, 2021. https://doi.org/10.1016/j.jor.2021.04.004

[8] Nawaz Khan, A., Gupta, M., Mahajan, P., Das, A., and Alagirusamy, R. " UHMWPE textiles and composites, " Textile Progress, Vol. 53, No. 4, pp. 183-335, 2022. https://doi.org/10.1080/00405167.2022.2087400

[9] Kluess, D., Martin, H., Mittelmeier, W., Schmitz, K.-P., and Bader, R. " Influence of femoral head size on impingement, dislocation and stress distribution in total hip replacement, " Medical Engineering & Physics, Vol. 29, No. 4, pp. 465-471, 2007. https://doi.org/10.1016/j.medengphy.2006.07.001

[10] Ipavec, M., Brand, R., Pedersen, D., Mavčič, B., Kralj-Iglič, V., and Iglič, A. " Mathematical modelling of stress in the hip during gait, " Journal of Biomechanics, Vol. 32, No. 11, pp. 1229-1235, 1999. https://doi.org/10.1016/S0021-9290(99)00119-0

[11] Berry, D. J., Von Knoch, M., Schleck, C. D., and Harmsen, W. S. " Effect of femoral head diameter and operative approach on risk of dislocation after primary total hip arthroplasty, " The Journal of Bone & Joint Surgery, Vol. 87, No. 11, pp. 2456-2463, 2005. https://doi.org/10.2106/JBJS.D.02860

[12] Sultan, P., Tav, V., Lai, M., and Garino, J. " Enhanced Stability of Total Hip Replacement Implants Resulting from Use of an Elevated-Rim Acetabular Liner and 32-mm Femoral Head, " University of Pennsylvania Orthopaedic Journal, Vol. 15, pp. 17-19, 2002.

[13] Morais, M. S., Bonfim, D. P., Aguiar, M. L., and Oliveira, W. P. " Electrospun poly (vinyl alcohol) nanofibrous mat loaded with green propolis extract, chitosan and nystatin as an innovative wound dressing material, " Journal of Pharmaceutical Innovation, Vol. 18, pp. 704-718, 2023. https://doi.org/10.1007/s12247-022-09681-7

[14] Urkaç, Ş. E. S. " Characterization of ultra high molecular weight polyethylene (UHMWPE) modified by metal-gas hybrid ion implantation technique, " MSc Thesis, Izmir Institute of Technology, Turkey, 2006.

[15] ASTM International. ASTM G99-17: Standard Test Method for Wear Testing with a Pin-on-Disk Apparatus, American Standard for Testing and Materials, 2017.

[16] Zhang, Z., and Ren, S. " Functional gradient ultrahigh molecular weight polyethylene for impact-resistant armor, " ACS Applied Polymer Materials, Vol. 1, No. 8, pp. 2197-2203, 2019. https://doi.org/10.1021/acsapm.9b00456

[17] Thomas, L. V., Arun, U., Remya, S., and Nair, P. D. " A biodegradable and biocompatible PVA–citric acid polyester with potential applications as matrix for vascular tissue engineering, " Journal of Materials Science: Materials in Medicine, Vol. 20, pp. 259-269, 2009. https://doi.org/10.1007/s10856-008-3599-7

[18] Maizatul, N., Norazowa, I., Yunus, W., Khalina, A., and Khalisanni, K. " FTIR and TGA analysis of biodegradable poly (lactic acid)/treated kenaf bast fibre: Effect of plasticizers, " Pertanika Journal of Science and Technology, Vol. 21, No. 1, pp. 151-160, 2013.

[19] Ogata, N., Jimenez, G., Kawai, H., and Ogihara, T. " Structure and thermal/mechanical properties of poly (l- lactide)- clay blend, " Journal of Polymer Science Part B: Polymer Physics, Vol. 35, No. 2, pp. 389-396, 1997. https://doi.org/10.1002/(SICI)1099-0488(19970130)35:2%3C389::AID-POLB14%3E3.0.CO;2-E

[20] Wang, Z., Li, Q., Chen, X., Zhang, Q., and Wang, K. " High crystallinity makes excellent wear resistance in crosslinked UHMWPE, Polymer, " Vol. 280, p. 126059, 2023. https://doi.org/10.1016/j.polymer.2023.126059

[21] Hussain, M., Naqvi, R. A., Abbas, N., Khan, S. M., Nawaz, S., Hussain, A., Zahra, N., and Khalid, M. W. " Ultra-high-molecular-weight-polyethylene (UHMWPE) as a promising polymer material for biomedical applications: A concise review, " Polymers, Vol. 12, No. 2, p. 323, 2020. https://doi.org/10.3390/polym12020323

[22] Mao, X., Liao, S., Wu, M., and Wang, Z. " The relationship between the crystallization of UHMWPE/HDPE injection-molded products and their frictional and mechanical properties, " Polymer, Vol. 320, p. 128092, 2025. https://doi.org/10.1016/j.polymer.2025.128092

[23] Chuaponpat, N., Ueda, T., Ishigami, A., Kurose, T., and Ito, H. " Morphology, thermal and mechanical properties of co-continuous porous structure of PLA/PVA blends by phase separation, " Polymers, Vol. 12, No. 5, p. 1083, 2020. https://doi.org/10.3390/polym12051083

[24] Li, D., Zhang, S., Zhao, Z., Miao, Z., Zhang, G., and Shi, X. " High-expansion open-cell polylactide foams prepared by microcellular foaming based on stereocomplexation mechanism with outstanding oil–water separation, " Polymers, Vol. 15, No. 9, p. 1984, 2023. https://doi.org/10.3390/polym15091984

[25] Wang, H., Shao, Z., Shen, K., Bateer, B., Ren, F., and Qi, X. " Super Hydrophobic UHMWPE/PTFE/PVA Composites with Low Friction: Preparation and Wear Mechanism, " Polymers, Vol. 17, No. 12, p. 1664, 2025. https://doi.org/10.3390/polym17121664

[26] Huzni, S., Tanamas, M. I., Fonna, S., and Ariffin, A. " The Sensitivity Analysis in Topology Optimization of Hip Stem Prosthesis Using Finite Element Method, " IOP Conference Series: Materials Science and Engineering, Vol. 931, p. 012001, 2020. https://doi.org/10.1088/1757-899X/931/1/012001

[27] Di Puccio, F., and Mattei, L. " A novel approach to the estimation and application of the wear coefficient of metal-on-metal hip implants, " Tribology International, Vol. 83, pp. 69-76, 2015. https://doi.org/10.1016/j.triboint.2014.10.023

[28] Peng, Y., Arauz, P., An, S., and Kwon, Y.-M. " Computational modeling of polyethylene wear in total hip arthroplasty using patient-specific kinematics-coupled finite element analysis, " Tribology International, Vol. 129, pp. 162-166, 2019. https://doi.org/10.1016/j.triboint.2018.08.009

[29] Belwanshi, M., Jayaswal, P., and Aherwar, A. " Wear and fatigue behaviour investigation of hip implant head-stem interface using finite element analysis, " Materials Today: Proceedings, Vol. 56,No. 5 pp. 2893-2901, 2022. https://doi.org/10.1016/j.matpr.2021.10.188

[30] Duc, N. D., Quang, V. D., Nguyen, P. D., and Chien, T. M. " Nonlinear Dynamic Response of Functionally Graded Porous Plates on Elastic Foundation Subjected to Thermal and Mechanical Loads, " Journal of Applied and Computational Mechanics, Vol. 4, No. 4, pp. 245-259, 2018.

[31] Torres, Y., Trueba, P., Pavón, J., Chicardi, E., Kamm, P., García-Moreno, F., and Rodríguez-Ortiz, J. " Design, processing and characterization of titanium with radial graded porosity for bone implants, " Materials & Design, Vol. 110, pp. 179-187, 2016. https://doi.org/10.1016/j.matdes.2016.07.135

[32] Plank, J., Singleton, L., and Probst, M. Effect of Nordic Hamstring Exercise on Knee Flexor Torque in Female Athletes: A Pilot Study. 2025 Celebration of Student Scholarship - Poster Presentations, 2025.

[33] Liu, C., Wu, J., Li, J., Ren, L., Tong, J., and Arnell, A. " Tribological behaviours of PA/UHMWPE blend under dry and lubricating condition, " Wear, Vol. 260, No. 1-2, pp. 109-115, 2006. https://doi.org/10.1016/j.wear.2004.12.044

[34] Li, X., Zhou, W., and Jiang, T. " Preparation of UHMWPE/PLA blends, " China Synthetic Resin and Plastics, Vol. 25, pp. 11-15, 2008

[35] Plamadiala, I., Croitoru, C., Pop, M. A., and Roata, I. C. " Enhancing polylactic acid (PLA) performance: A review of additives in fused deposition modelling (FDM) filaments, " Polymers, Vol. 17, No. 2, pp. 191, 2025. https://doi.org/10.3390/polym17020191

[36] Yang, C., Zhang, J., Yue, H., and Kang, X. " The Low Friction Coefficient and High Wear Resistance UHMWPE: The Effect of Pores on Properties of Artificial Joint Materials, " Lubricants, Vol. 13, No. 1, p. 31, 2025. https://doi.org/10.3390/lubricants13010031